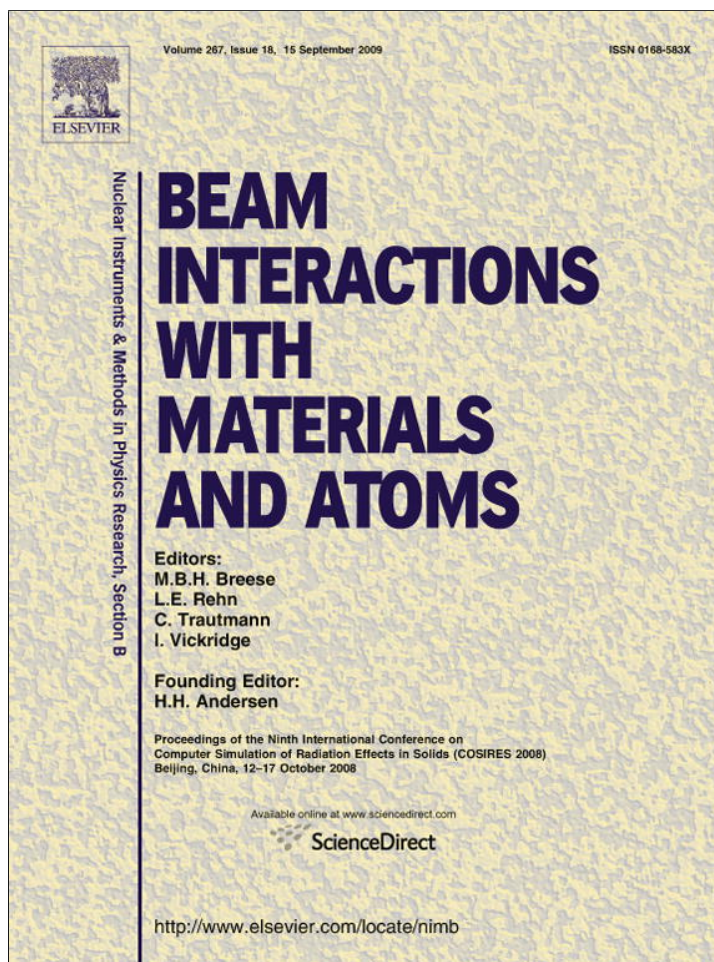


Provided for non-commercial research and education use.  
Not for reproduction, distribution or commercial use.



This article appeared in a journal published by Elsevier. The attached copy is furnished to the author for internal non-commercial research and education use, including for instruction at the authors institution and sharing with colleagues.

Other uses, including reproduction and distribution, or selling or licensing copies, or posting to personal, institutional or third party websites are prohibited.

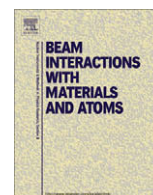
In most cases authors are permitted to post their version of the article (e.g. in Word or Tex form) to their personal website or institutional repository. Authors requiring further information regarding Elsevier's archiving and manuscript policies are encouraged to visit:

<http://www.elsevier.com/copyright>



Contents lists available at ScienceDirect

## Nuclear Instruments and Methods in Physics Research B

journal homepage: [www.elsevier.com/locate/nimb](http://www.elsevier.com/locate/nimb)

## Transition from atomistic to macroscopic cluster stopping in Au

Juha Samela\*, Kai Nordlund

Department of Physics, University of Helsinki, P.O. Box 43, FI-00014 Helsinki, Finland

## ARTICLE INFO

## Article history:

Available online 17 June 2009

## PACS:

79.20.-m

61.80.jh

83.10.Rs

## Keywords:

Cratering

Cluster ion impact

Molecular dynamics

## ABSTRACT

Based on large-scale molecular dynamics simulations of Au cluster impacts on a Au surface, we have recently reported that the transition to macroscopic crater volume scaling behavior occurs between 1000 and 100,000 Au atoms at impact velocities comparable to typical meteoroid velocities [J. Samela, K. Nordlund, Atomistic simulation of the transition from atomistic to macroscopic cratering, Phys. Rev. Lett. 101 (2008) 027601]. Now we have analyzed the conditions that lead to this transition in more detail. The main mechanisms of this change is the emergence of the transient high-density region which can store two thirds of the impact energy. This mechanism becomes the dominant cratering mechanisms gradually when the impactor size increases.

© 2009 Elsevier B.V. All rights reserved.

## 1. Introduction

The stopping mechanisms of small clusters at velocities smaller than the Bohr velocity are now well understood in Au [1,2], in crystalline Si [3,4], in amorphous Si [5], and in many other types of targets [6–10]. A characteristic feature of these small-scale impacts is the non-linear cluster size dependence of many quantities like sputtering yield and crater volume [11]. On the other hand, impacts of macroscopic objects are studied in the contexts of materials engineering [12], large meteoroid impacts on planetary surfaces, micrometeoroid impacts on spacecraft [13,14], and other kinds of impacts in space [15,16]. In these impacts, the crater volume scales linearly with impactor size [17]. Thus, the transition from non-linear to linear behavior occurs at cluster sizes between those typical in nanoscience and sizes studied in planetary science. Increasing performance of parallel-computing provides an opportunity to explore this transition region now with molecular dynamics simulations [18].

Based on large-scale molecular dynamics simulations of Au cluster impacts on a Au surface, we have recently reported that the transition to macroscopic scaling behavior occurs between 1000 and 100,000 Au atoms at impact velocities comparable to typical meteoroid velocities [19]. Now we have analyzed the conditions that lead to this transition in more detail.

Cluster ion beam techniques are continuously developing and larger clusters can be produced [6]. Atomic cluster impacts that have some characteristic of macroscopic impacts become eventu-

ally possible in laboratories. To predict their applications on surface processing, a good understanding of effects of single impacts are first needed. The purpose of this study is to understand the stopping mechanisms of large atomic cluster ions in Au. We have chosen an fcc metal because metals are among the most simple systems which are available for experimental impact studies. Among the fcc metals, Au is chosen because the results can be compared to previous small cluster studies [1,2].

In the theory of planetary impact processes, an approximation is made: the impact energy is assumed to be instantaneously deposited in a region of zero extent inside the target [17]. This approximation is based on the observations that macroscopic impact usually occur at two phases. In the first phase, the impactor, together with some target material, is compressed in a small volume where the energy density is very high. Then this energy is released almost radially and a crater is formed. The high-density region is also called an isobaric core [20]. Because most of the impact energy is first stored in the core and only then released, the scaling of crater volume is linear [17].

In this study, we focus on analysis of formation and development of a high-pressure core at different energies and cluster sizes. It will be shown, that the approximation of a spherical isobaric core or even a core with zero extent becomes appropriate when both impactor size and energy increases.

## 2. Methods

Cluster ion impacts were simulated with classical molecular dynamics (MD) employing many-body interatomic potentials

\* Corresponding author.

E-mail address: [juha.samela@helsinki.fi](mailto:juha.samela@helsinki.fi) (J. Samela).

implemented in the PARCAS MD code. The main principles of the molecular dynamics algorithms are presented in [21,22]. The adaptive time step and electronic stopping algorithms are the same as in [23]. The interaction model used in the simulations was the molecular dynamics and Monte Carlo corrected effective medium model (MD/MC-CEM) [24,25]. A short-range repulsive force [26] was also present to better describe collisions of Au atoms.

In the simulations, an Au(111) surface was bombarded with  $Au_N$  clusters,  $N = 55, 750, 6300, 68,000$ . The impact velocities were chosen to be comparable to the hypervelocity regime typical for micrometeoroid impacts [27]. The velocities were 2.2, 7.0, 22.1, and 70.0 km/s corresponding to kinetic energies 5, 50, 500, and 5000 eV/atom, respectively. In addition to the normal incident angle, also 20°, 40°, and 60° oblique angles were simulated.

The clusters were created by first cutting appropriate volumes from a relaxed Au fcc crystal and then stabilizing the clusters with MD at 100 K, which was the ambient temperature of the simulations. The  $Au_{68,000}$  was almost cubic and others were spherical. In addition, disc-shaped and cigar-shaped ellipsoids were used. The inner structure in all clusters were fcc, thus the density of the clusters were the same as the Au(111) density. The impact points were chosen randomly.

To study the compression mechanisms it was sufficient to simulate only the stopping phase. The simulations were stopped before the deformations or shock waves reached the boundaries of the simulation box. The simulation times were 1–5 ps depending on the impact energy and cluster size. The Au(111) target was 13 nm wide and contained approximately one million atoms. To simulate the full cratering events, considerably larger targets and longer simulation times must be used [19]. For example, a full simulation of 5 keV/atom  $Au_{68,000}$  impact would require a target of 500 million atoms and 400 ps simulation time.

In large cluster impact simulations, one simulated case is usually enough to give a reasonable estimate for many quantities like crater size because the atomic level random behavior affects only slightly on the average coherent movements of atoms. However, we simulated three cases of normal incident spherical cluster impacts at each velocity and cluster size to find out the magnitude of statistical variation.

Atomic densities were calculated for each atom by counting the number of neighbors of the atom in a surrounding sphere whose

volume is  $1 \text{ nm}^3$ . This method gives density fields that describe the high-density regions more accurately than the average densities calculated in cubic cells of a grid.

### 3. Results

#### 3.1. Stopping process

A typical chain of events of cluster stopping is shown in Fig. 1. The cluster atoms sharply lose most of their velocity in collisions with the substrate atoms and with the foremost cluster atoms at the surface of the substrate. The cluster is gradually compressed and it forms a clear high-density region where atoms have high potential energy. In this study, densities up to 3.5 times higher than the normal Au density have been detected but higher densities are possible. The core grows from both sides: also the substrate atoms beneath the core join it. This compressing stopping mechanism is clearly different from the mechanism in small cluster impacts, where the cluster atoms more or less penetrate between the substrate atoms or can even channel at high energies [2]. At large cluster sizes, two mechanisms block the cluster to penetrate into the substrate. Firstly, the frontier of cluster atoms is so wide that the substrate atoms can not escape the frontier because the crystal blocks their motion. Secondly, the first frontier of cluster atoms collide with the substrate atoms and lose most of their velocity, forming a barrier that almost completely stops other cluster atoms that follow the first frontier. This mechanism is called the piling-up effect.

The compression continues and density increases until the entire cluster is smashed. In this phase (300 fs in Fig. 1), the cluster is compressed beneath the original surface and only a few atoms are sputtered. During the smashing phase and sometime after that, the high-density region continues its movement inside the substrate leaving a cavity behind. This is called the sinking effect. The high-density region has the shape of a bowl. The reason to that is seen in Fig. 1. The movement into the deeper parts of the substrate is stronger in the direction of the cluster, but the frontier spreads at the same time because of the high potential energy it contains. Finally, when the frontier has weakened and decelerated, it can not destroy the substrate structure any more. The frontier becomes a series of shock waves which distribute a portion of

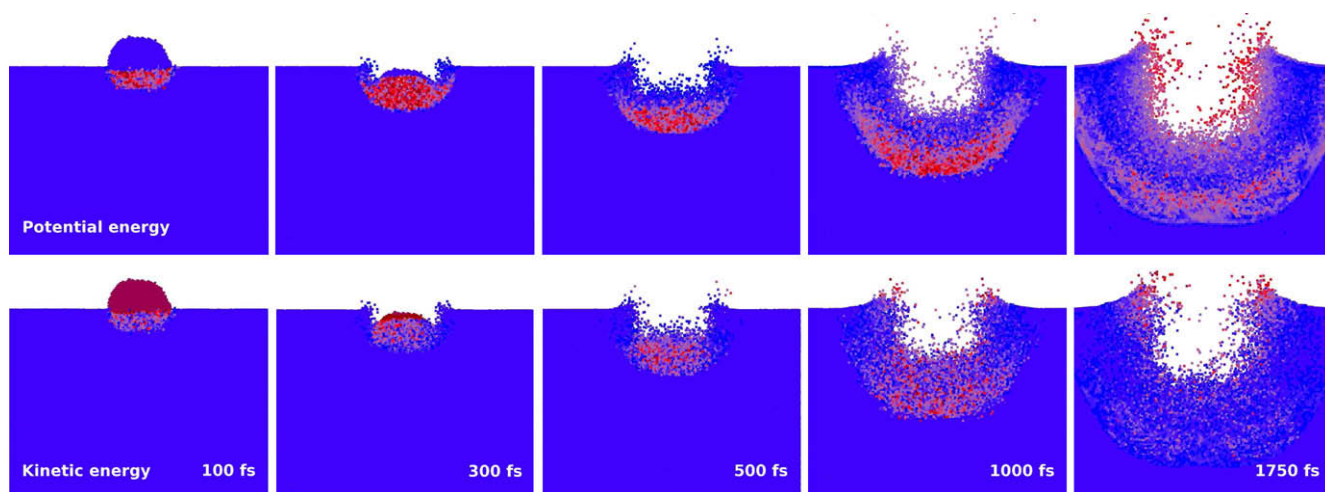


**Fig. 1.** An example of energy distribution in a 5 keV/atom  $Au_{6300}$  impact. Upper row shows development of the potential energy field at 100, 300, 500, 1000, and 1750 fs after the border of the cluster has reached the Au(111) surface. Potential energy is high in the high-density regions. The lower row shows the corresponding kinetic energy distributions. High energy areas are red (light in grayscale copy). Notice that in this figure, the energy that is rendered in red varies between the frames in order to show the geometry of the energy distribution at each phase clearly, in other words, the red shades are not comparable between the frames. (In other figures, scales are not varied between frames.) The frames are 27 nm wide. (For interpretation of the references to color in this figure legend, the reader is referred to the web version of this article.)

the impact energy deeper into the substrate. The shock waves are not spherical because their shape is deformed according to the crystal structure.

The cavity that the high-density region leaves behind is not the final crater. The process has left energy in the walls of the cavity, thus the melting of substrate continues a relatively long time after the cavity formation and a crater larger than the initial cavity is formed [19,2].

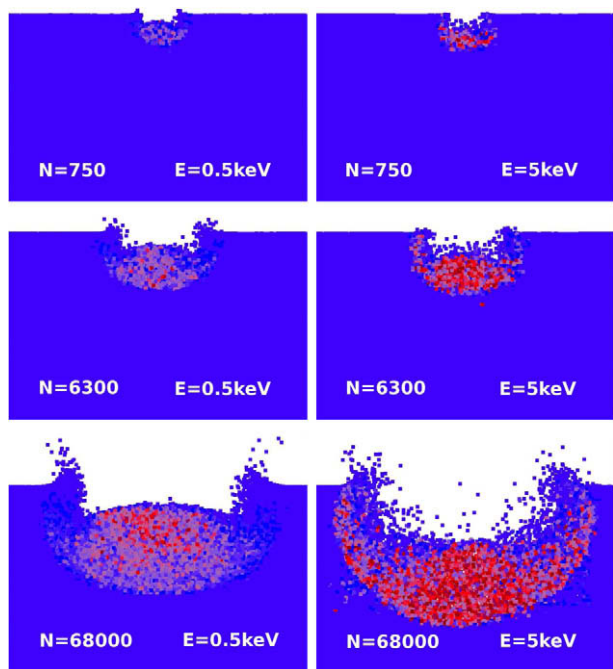


Fig. 2. Comparison of high-pressure regions at the moment when the clusters are smashed and before the expansions starts. High potential energy areas are red (light in grayscale copy), the maximum being 76 eV/atom. The left column shows 500 eV/atom events and the right column 5 keV/atom events. The frames are 27 nm wide. (For interpretation of the references to color in this figure legend, the reader is referred to the web version of this article.)

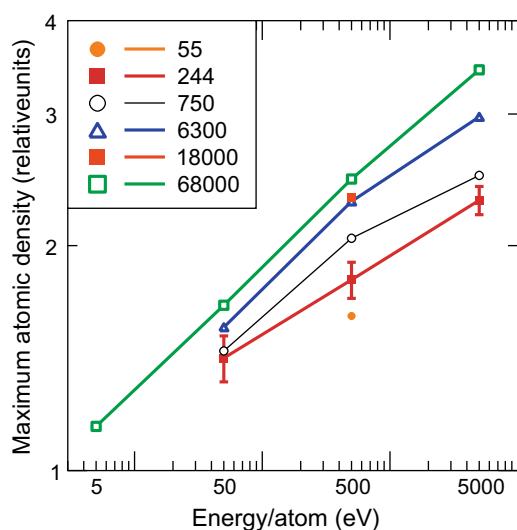


Fig. 3. Atomic density as a function of impactor size (atoms) and impact velocity (kinetic energy/atom). The density is given relative to the normal Au atomic density (69 atoms/nm<sup>3</sup>).

### 3.2. Effect of impactor size and velocity

Fig. 2 shows the forms of high-pressure regions at three different impactor sizes and two impact velocities. When the number of atoms in the cluster increases, the piling-up lasts longer. Therefore, the atomic density becomes higher. The 500 eV/atom Au<sub>6300</sub> event in Fig. 2 shows the effect of pile-up on density distribution: The density is higher in the upper parts of the compressed region. On the other hand, when the impact velocity increases, the compression is stronger but it lasts a shorter time. Then the sinking of the high-density region is faster.

Fig. 3 verifies quantitatively these observations. Both impactor size and impact velocity increases the maximum density. The maximum density  $d_{\max} \propto N^a$ , where  $a = 0.06 \pm 0.01$ . If we assume that the effect of the pile-up would depend linearly on the cluster diameter, then the relation should be  $d_{\max} \propto N^{1/3}$ , which is clearly not true. The density depends on impact energy in an even more complicated way. At  $N = 68,000$  the relation is a power law  $d \propto E^b$ , where  $b \approx 0.157 \pm 0.004$ . At smaller cluster sizes, the density increases slower at high velocities because of a kind of clearing-the-way effect: A considerable portion of the substrate atoms escape the core because the forces are high enough to induce this movement. The larger the cluster, the higher the velocity needed for this clearing-the-way effect to occur (Fig. 3). At sizes and velocities that do not produce the clearing-the-way effect, we can approximate that in the hypervelocity regime the relative maxi-

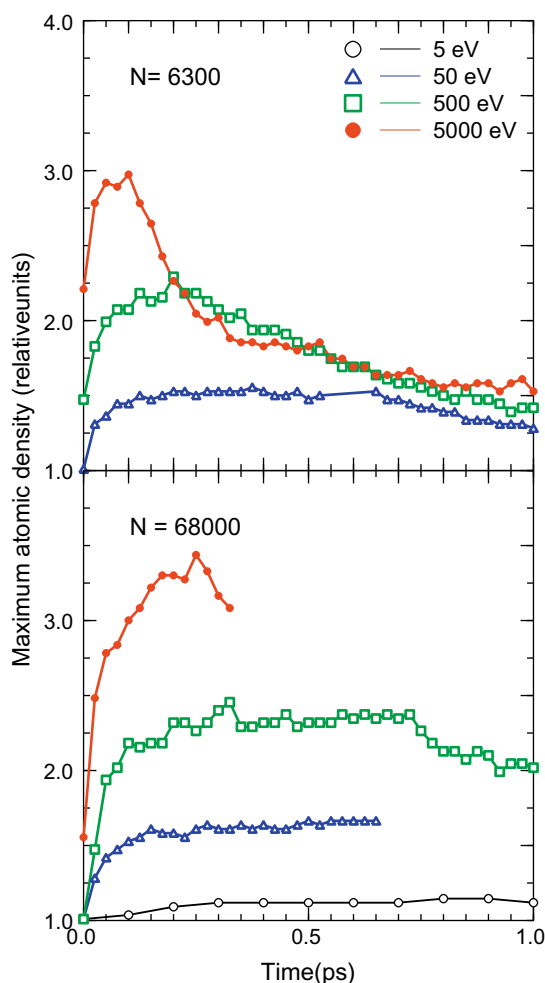


Fig. 4. Maximum relative density as a function of time after the border of the cluster has hit the original surface.

imum density  $d_{\max}$  depends on impact energy per atom  $E$  and cluster size  $N$  in the following way:

$$d_{\max} \propto N^a E^b, \quad (1)$$

where  $a$  and  $b$  are material dependent parameters. At the transition region, the scaling is more complicated.

### 3.3. Evolution of the high-density region

As discussed in Section 3.1, the high-density region develops during the piling-up phase and then spreads while moving deeper into the substrate. Fig. 4 shows the dynamics of maximum relative density as a function of time. The absolute maximum occurs approximately at the end of the piling-up. After that the density begins to decrease.

Fig. 5 shows at which depth the highest density is located as a function of time. In general, the highest density occurs near the surface until the piling-up is over. Figs. 4 and 5 indicate that after the piling-up phase the point of maximum density moves away from the surface at constant velocity (sinking effect), which depends on the impact size more than impact velocity. The core occurs deeper in the substrate when the impact energy increases, which is also the case in the macroscopic impacts [20].

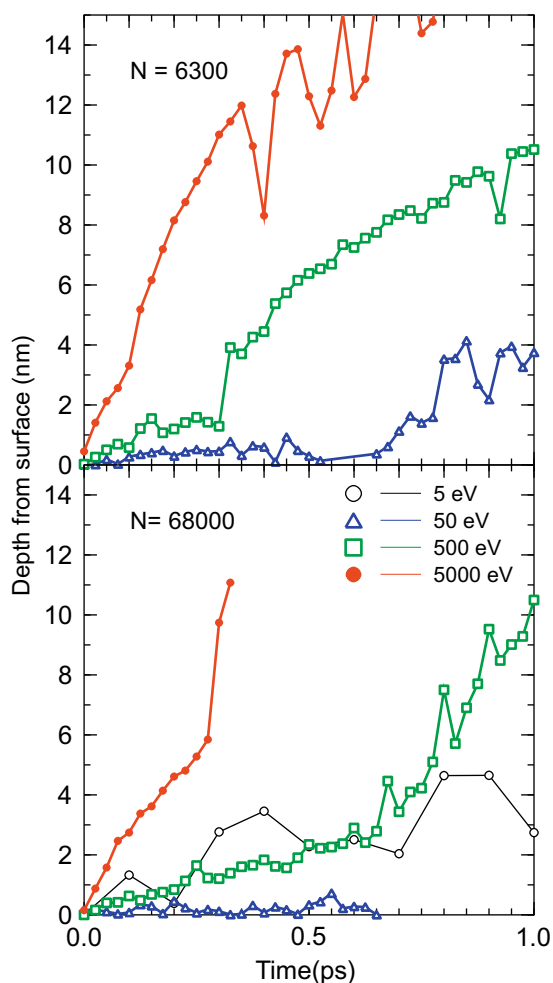


**Fig. 5.** The depth of occurrence of the maximum density as a function of time. The maximum density varies over time, and the absolute maximum is reached in relatively early phase (Fig. 4) when the cluster is piled up in the bottom of the cavity. After that, the high-density core continues its penetration deeper into the substrate in almost constant velocity. At 5 eV/atom, the location of the maximum density does not always occur in the center of core because strong shock waves are induced from the core (Fig. 8).

### 3.4. Energy distribution

The high-density core is a transient energy storage between the stopping and expansion phases of the collision process (Fig. 1). Both kinetic and potential energy is high in the core. Fig. 6 shows how the core develops over time. During the piling-up phase, a very dense core develops and it has high potential energy. The density decreases when the core is expanding and the potential energy decreases, too.

The potential energy maximum occurs approximately when the pile up phase is over, in coincidence with the density maximum. Fig. 7 shows that the maximum per cluster size  $N$  is relatively constant when  $N \geq 244$ . Therefore, it is not possible to predict the potential energy directly according to the maximum density because the maximum density depends non-linearly on impactor size (Eq. (1)).

At 500 eV/atom, only 10–12% of the impact energy is stored in the high-energy region as a form of potential energy despite of

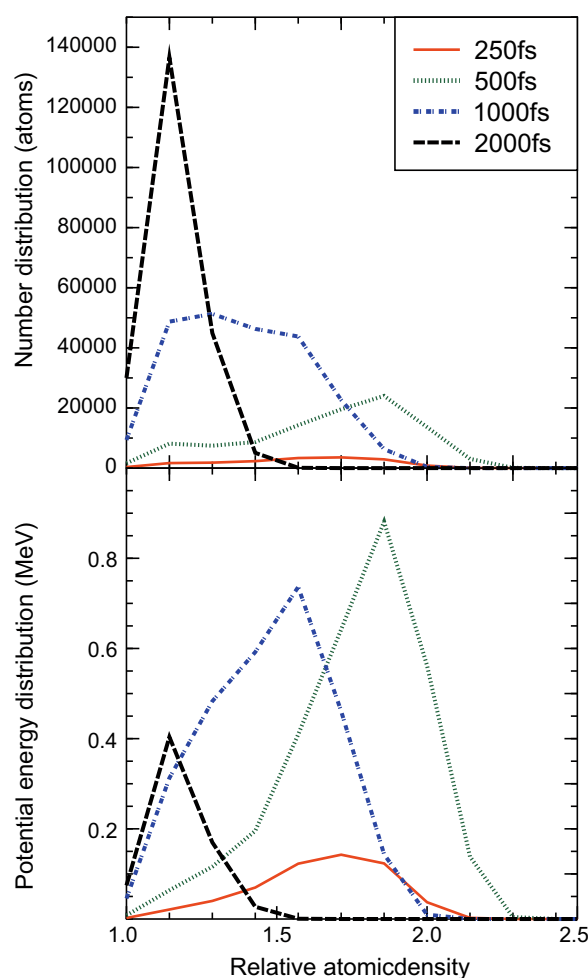


**Fig. 6.** The upper frame shows how many atoms are located in high density core after 500 eV/atom  $Au_{68,000}$  impact (34 MeV total). More precisely, the relative number density is higher than 1.0, if the atom has more neighbor atoms than atoms in crystalline Au inside a surrounding sphere whose volume is  $1 \text{ nm}^3$ . The bin width of the distribution is 0.1. The lower frame shows how much potential energy these atoms have in total. For example, at 2000 fs and at relative density of 1.1 the number of atoms is almost 140,000 and their total potential energy is 0.4 MeV. The corresponding average potential energy per atom is 2.9 eV. At the densest parts of the core, potential energy per atom is more than 10 times higher. Thus, relatively small number of atoms act as a transient storage of energy between cluster stopping and displacement cascade expansion phases. The distributions are averages of three simulated events.

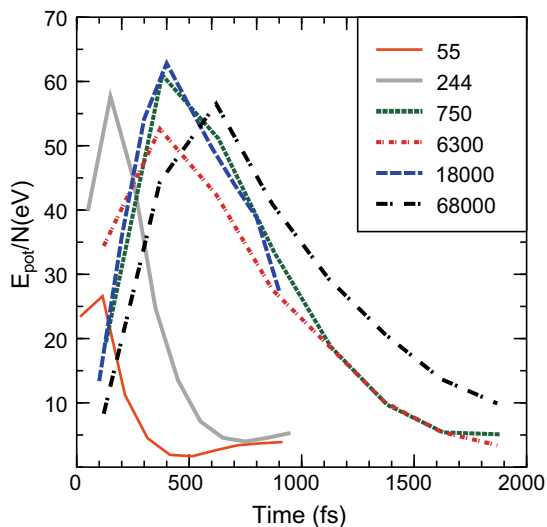


**Fig. 7.** Potential energy per  $N$  stored in the high-density region as a function of time. The results are averages over three simulations. The impact energy is 500 eV/atom.

the high density. Thus, the kinetic energy of the core is larger than its potential energy. In addition to the random motion of core atoms, the core moves coherently deeper into the substrate and also expands laterally. Therefore, the kinetic energy has a random and a coherent component. At its maximum, the total core energy is more than  $2/3$  of the impact energy when  $N \geq 750$ . This ratio is also almost independent of  $N$ . Thus, the stored energy depends linearly on  $N$ . Because the final crater is a result of distribution of this energy, this is consistent with the fact that also the final crater volume depends linearly on  $N$ , which is verified by MD simulations [19]. However, the linear scaling of the core energy occurs at much smaller cluster sizes than the linear scaling of crater volumes.

The core energy is released in many ways. Fast atoms are sputtered from the surface of the core immediately after the core pile-

up is over. However, most of the energy is released from the core as it expands and melts the surrounding structure. Sputtered atoms and clusters carry a considerable portion of the energy away from the cavity during and after the expansion. At the end of the expansion process, shock waves are induced and they distribute energy deeper into the substrate. The energy distribution is not quantitatively analyzed here because only the stopping phase is simulated. At high energies of 5 keV/atom, channeling of atoms from the surface of the core weakens the compression, but the effect is very small.

### 3.5. Low energy impact, oblique angles and deformed clusters

**Fig. 8** shows an example of 5 eV/atom event where shock waves are induced already during the pile-up phase. The impact velocity is 2.2 km/s which is less than 3.24 km/s, the velocity of sound in Au. Because shocks can induce structural modifications, we can expect that these sub-sonic impacts have different structural effects than super-sonic impacts.

A high-density core emerges also at oblique incident angles (**Fig. 9**). When the angle increases, the core becomes asymmetric. At large angles, a flow of atoms away from the cavity is induced already during the pile up, which probably effects sputtering yield. At even larger angles, it is possible that the cluster will be fragmented and parts of it are scattered. This is observed experimentally in macroscopic impacts [28]. Fullerenes can scatter from the surface at glancing angles [29].

The shape of the cluster affects the shape of the core (**Fig. 9**). Ellipsoidal clusters induce different core shapes depending on their orientation and how oblong they are. The high-density region is located deeper when more atoms are piled up. On the other hand, the  $\text{Au}_{68,000}$  clusters simulated in this study were cubic with rounded corners. They induced symmetric cores and final craters [19]. In conclusion, the core shape changes only when the clusters are clearly ellipsoidal or the spherical symmetry is broken in some other way.

## 4. Discussion

The results show that the transient high-density core emerges already at relatively small impactor sizes but the macroscopic scaling of crater volume is reached only when the impacting Au cluster has more than around 50,000 atoms [19]. At small cluster sizes and at the energies comparable those used in this study, the crater is formed mainly due to heating of the collision cascade region and its surroundings and due to the consequent flow of atoms to vacuum [30–33]. At larger cluster sizes, a cavity is first formed during the cluster stopping phase and then the impact energy stored in the high-density core in the bottom of the cavity is released beneath the initial surface. The sinking core induces the final crater. The later cratering process becomes dominant over the collision cascade cratering process gradually when impactor size increases.

At a given impact velocity, the total energy per cluster size  $N$  stored in the high-density region is almost constant. In other words, the kinetic energy of the cluster is mostly gained by the high-density region which moves deeper into the substrate in direction of the incident cluster motion (**Fig. 9**). However, the linear scaling of the core energy begins at  $N < 500$  while the linear scaling of crater volumes begins only when  $N > 50,000$ . The sinking depth depends on both impact velocity and impactor size. When the cluster is large enough the energy is released clearly beneath the surface and the melted volume depends linearly on the energy of the high-density region. This leads to the macroscopic scaling behavior. At the transition region where  $N = 100\text{--}50,000$ , the collision cascade cratering process, which induces non-linear scaling,

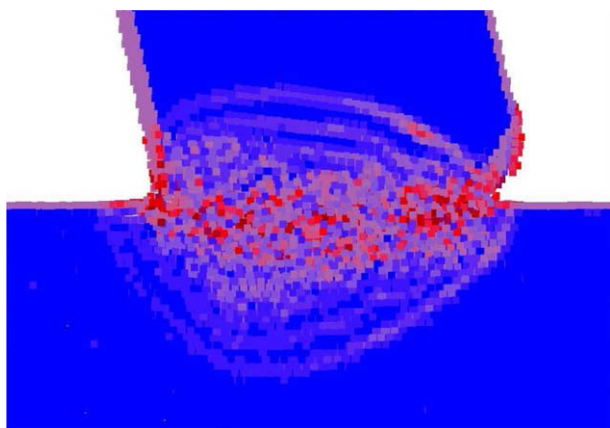


**Fig. 8.** A non-perspective side view through the cut target crystal and impacting cluster during a stopping phase of 5 eV/atom  $\text{Au}_{68,000}$  impact. Red color (light areas in grayscale) show high potential areas relative to the atomic potential in crystalline Au. A series of weak shock waves are induced during the stopping phase, which are shown as red (light) frontiers moving either through the target crystal or through the impacting cluster. The surface layers are also shown in red (light gray) because of the different atomic potential at surface. This indicates that the potential in the shock waves in this case has the magnitude of surface energy. In the other side views in this article, potential differences at surfaces are not shown because the color scales used in visualizations are different. (For interpretation of the references to color in this figure legend, the reader is referred to the web version of this article.)

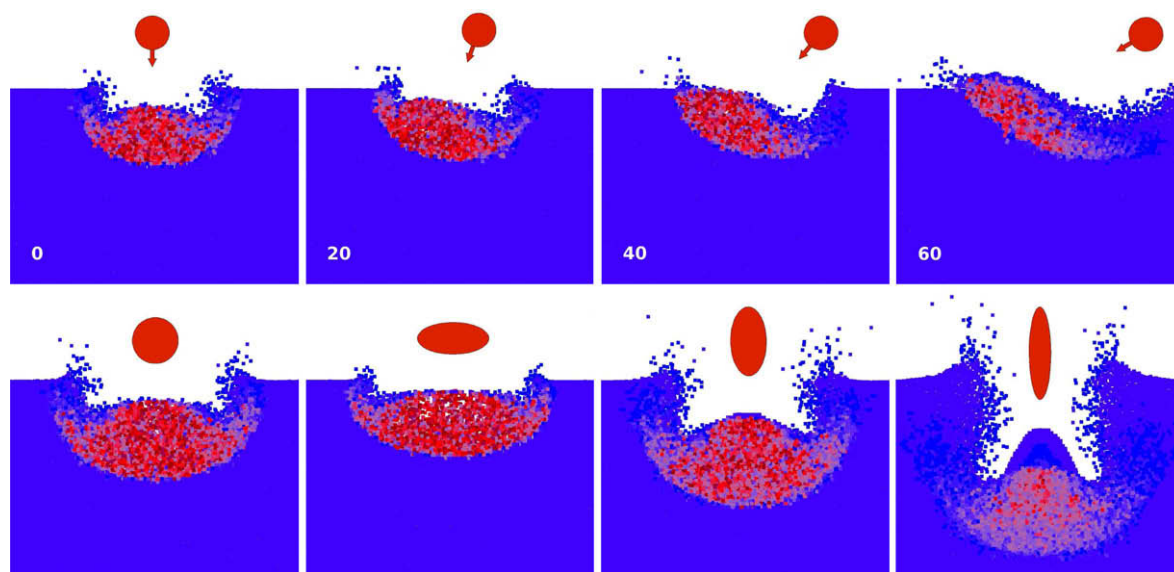


**Fig. 9.** Upper row: examples of high-density core shapes at different incident angles ( $\text{Au}_{6300}$ , 500 eV/atom). Lower row: effect of cluster shape on core shape ( $\text{Au}_{18,000}$ , 500 eV/atom). The leftmost cluster is spherical.

and macroscopic cratering process compete. This explains the gradual transition of crater volume scaling from non-linear to linear scaling in [19]. The crater volume  $V/N$  is smaller at the macroscopic cratering regime because a considerable portion of the energy is converted to shock wave energy and heat. At small cluster size, a larger portion of the energy is removed from the cavity by the sputtered atoms.

The pile-up is clearly a size-dependent effect, therefore we expect that it occurs in every dense substrate regardless of its crystal structure or whether the substrate is amorphous or crystalline. The densities of materials affect the scaling parameters [17].

High-density region is not spherical nor is it isobaric, as it is approximated in hydrodynamical models of macroscopic impacts [20]. However, the isobaric approximation works in practice because the energy release from the compressed region is almost radial. However, at the transition sizes  $N = 100\text{--}50,000$ , the isobaric core approximation is not valid, because several ejection mechanisms effect the crater formation.

Anders and Urbassek have recently studied the clearing-the-way effect of small and medium-size Au clusters ( $N = 1\text{--}402$ ) [1]. They found that the cluster stopping is reduced by a factor  $N^\beta$ , where  $\beta = 0.7$  at 1 keV/atom. This result is consistent with our finding that the cavity becomes deeper when  $N$  increases due to the sinking and clearing-the-way effects.

It is possible to produce Au clusters at sizes and energies comparable to those used in this study [34]. However, no experimental data is currently available to verify the results of simulations, like crater volumes and sputtering yields. However, the crater volume scaling is similar to the macroscopic scaling and the high-density core is in agreement with the process known to exist in macroscopic impacts.

Finally, we bring up two issues about the molecular dynamics method. The repulsive part of the potentials used in the bombardment simulations are valid at short distances and the repulsion between two atoms can be modeled correctly. However, the interaction potentials available are usually not intended to describe many-atom interactions of materials that have 2–4 times the normal density. It is impossible to verify how much this may affect the results because the lack of experimental data. We believe that the effect is very small to crater scaling because most of the interactions that lead to crater formation occur at almost normal

densities. The second thing about the methodology is the number of simulations required for reliable averages. The results show that even one simulated event of large cluster impact gives very good estimates of quantities that are results of coherent behavior, for example quantities like cavity depth, potential energy of the high-density region, and crater volume. However, some effects show random variation, which must be averaged over several simulations. Examples are coherent displacements around the cavity and defects induced by shock waves.

## 5. Conclusions

We have simulated the stopping phase of  $\text{Au}_N$ ,  $N = 55\text{--}68,000$  clusters on Au(111) surface at energies 5–5000 eV/atom. The simulations show that the linear scaling of crater volume with the impactor mass emerges when the impact energy is first stored in a small high-density region inside the substrate and then released radially. The compression of material occurs, when the impactor size is large enough to prevent the collision cascade to release its energy to the vacuum during the early phases of cascade development and the impact velocity high enough to cause the sinking of high-density core deeper inside the substrate.

The effect of impactor geometry and incident angle on the compression mechanism are also investigated. When the incident angle increases up to 30–40 degrees, the lateral effects become important. Small deviations from perfect spherical form of the cluster do not effect the compression mechanism. However, impacts of thin disks and rod-like objects give different results than spherically symmetric clusters of the same size.

The results explain the transition to the macroscopic crater scaling consistently with predictions of macroscopic impact theories. Similar mechanisms probably occur in all dense materials. Further investigations are welcome to find out possible applications of large atomic cluster impacts.

## Acknowledgements

We thank Dr. E.M. Bringa for useful discussions. This work was performed within the Finnish Centre of Excellence in Computational Molecular Science (CMS), financed by The Academy of Finland and the University of Helsinki. Grants of computer time

from the Center for Scientific Computing in Espoo, Finland, are gratefully acknowledged.

## References

- [1] C. Anders, H.M. Urbassek, Nonlinear stopping of heavy clusters in matter: a case study, *Nucl. Instr. and Meth. Phys. Res. B* 258 (2007) 497.
- [2] J. Samela, K. Nordlund, Origin of nonlinear sputtering during nanocluster bombardment of metals, *Phys. Rev. B* 76 (2007) 125434.
- [3] A. Titov, A. Azarov, L. Nikulina, S. Kucheyev, Damage buildup and the molecular effect in Si bombarded with pfn cluster ions, *Nucl. Instr. and Meth. Phys. Res. B* 256 (2007) 207.
- [4] J. Matsuo, S. Ninomiya, Y. Nakata, K. Ichiki, T. Aoki, T. Seki, Size effect in cluster collision on solid surfaces, *Nucl. Instr. and Meth. Phys. Res. B* 257 (2007) 627.
- [5] J. Samela, K. Nordlund, Emergence of non-linear effects in nanocluster collision cascades in amorphous silicon, *New J. Phys.* 10 (2008) 023013.
- [6] V.N. Popok, E.E.B. Campbell, Beams of atomic clusters: effect on impact with solids, *Rev. Adv. Mater. Sci.* 11 (2006) 19.
- [7] J.P. de Souza, M. Behar, J.F. Dias, J.H.R. dos Santos, Range parameters of  $^{18}\text{O}$  implanted into Si and  $\text{SiO}_2$ , *Nucl. Instr. and Meth. Phys. Res. B* 175 (2001) 46.
- [8] Y. Takahashi, T. Hattori, N. Hayashizaki, Energy loss of slow carbon cluster ions in thin carbon foils, *Phys. Rev. A* 75 (2007) 013202.
- [9] S. Harper, K.D. Krantzman, Molecular dynamics simulations to explore the role of mass matching in the kev bombardment of organic films with polyatomic projectiles, *Appl. Surf. Sci.* 231 (2004) 44.
- [10] J. Samela, K. Nordlund, V.N. Popok, E.E.B. Campbell, Origin of complex impact craters on native oxide coated silicon surfaces, *Phys. Rev. B* 77 (2008) 075309.
- [11] S. Bouneau, A. Brunelle, S. Della-Negra, J. Depauw, Y.L.B.D. Jacquet, M. Pautrat, M. Fallavier, J.C. Poizat, H.H. Andersen, Very large gold and silver sputtering yields induced by keV to MeV energy Au clusters ( $n = 1-13$ ), *Phys. Rev. B* 65 (2002) 144106.
- [12] T. Kadono, J. Kameda, K. Saruwatari, H. Tanaka, S. Yamamoto, A. Fujiwara, Surface roughness of alumina fragments caused by hypervelocity impact, *Planet. Space Sci.* 54 (2006) 212.
- [13] A. Kearsley, G. Graham, Multi-layered foil capture of micrometeoroids and orbital debris in low earth orbit, *Adv. Space Res.* 34 (2004) 939.
- [14] Y. Michela, J.-M. Chevalier, C. Durin, C. Espinosa, F. Malaise, J.-J. Barrau, Hypervelocity impacts on thin brittle targets: experimental data sph simulations, *Int. J. Impact Eng.* 33 (2006) 441.
- [15] E. Schneider, F. Schafer, Hypervelocity impact research – acceleration technology and applications, *Adv. Space Res.* 28 (9) (2001) 1417.
- [16] E.M. Bringa, R.E. Johnson, A new model for cosmic-ray ion erosion of volatiles from grains in the interstellar medium, *Astrophys. J.* 603 (2004) 159.
- [17] K.A. Holsapple, The scaling of impact processes in planetary sciences, *Annu. Rev. Earth Planet. Sci.* 21 (1996) 333.
- [18] C. Zhang, R.K. Kalia, A. Nakano, P. Vashishta, Fracture initiation mechanisms in alumina under hypervelocity impact, *Appl. Phys. Lett.* 91 (2007) 121911.
- [19] J. Samela, K. Nordlund, Atomistic simulation of the transition from atomistic to macroscopic cratering, *Phys. Rev. Lett.* 101 (2008) 027601.
- [20] E. Pierazzo, A.M. Vickery, H.J. Melosh, A reevaluation of impact melt production, *Icarus* 127 (1997) 408.
- [21] K. Nordlund, M. Ghaly, R.S. Averback, M. Caturla, T.D. de la Rubia, J. Tarus, Defect production in collision cascades in elemental semiconductors fcc metals, *Phys. Rev. B* 57 (13) (1998) 7556.
- [22] M. Ghaly, K. Nordlund, R.S. Averback, Molecular dynamics investigations of surface damage produced by kev self-bombardment of solids, *Phil. Mag. A* 79 (4).
- [23] K. Nordlund, Molecular dynamics simulation of ion ranges in the 1–100 keV energy range, *Comput. Mater. Sci.* 3 (1995) 448.
- [24] J.D. Kress, A.E. DePristo, Corrected effective medium method. ii.  $n$ -Body formulation, *J. Chem. Phys.* 88 (1988) 2596.
- [25] C.L. Kelchner, D.M. Halstead, N.M.W.L.S. Perkins, A.E. DePristo, Construction and evaluation of embedding functions, *Surf. Sci.* 310 (1994) 425.
- [26] J.F. Ziegler, J.P. Biersack, U. Littmark, *The Stopping and Range of Ions Matter*, Pergamon, NY, USA, 1985.
- [27] V. Jantou, D. McPhail, R. Chater, A. Kearsley, Analysis of simulated hypervelocity impacts on a titanium fuel tank from the SALYUT 7 space station, *Appl. Surf. Sci.* 252 (2006) 7120.
- [28] D.L. Orphal, Explosions and impacts, *Int. J. Impact Eng.* 33 (2006) 496.
- [29] R.P. Webb, The computer simulation of energetic cluster-solid interactions, *Radiat. Effects Def. Solids* 162 (7-8) (2007) 567.
- [30] M.M. Jakas, E.M. Bringa, Thermal-spike theory of sputtering: the influence of elastic waves in a one-dimensional cylindrical spike, *Phys. Rev. B* 62 (1999) 824.
- [31] M.M. Jakas, E.M. Bringa, R.E. Johnson, Fluid dynamics calculation of sputtering from a cylindrical thermal spike, *Phys. Rev. B* 65 (2002) 165425.
- [32] A. Brunelle, S. Della-Negra, Trends to a semi-empirical model for cluster induced metal sputtering, *Nucl. Instr. and Meth. Phys. Res. B* 222 (2004) 68.
- [33] M.R. Russo, B.J. Garrison, Mesoscale energy deposition footprint model for kiloelectronvolt cluster bombardment of solids, *Anal. Chem.* 78 (2006) 7206.
- [34] G. Hager, C. Guillermier, S. Verkhoturov, E. Schweikert, Au-analyte adducts resulting from single massive gold cluster impacts, *Appl. Surf. Sci.* 252 (2006) 6558.